Catalysis Science & Technology

ROYAL SOCIETY OF CHEMISTRY

PAPER

View Article Online
View Journal | View Issue

Check for updates

Cite this: *Catal. Sci. Technol.*, 2022, 12, 6231

A novel thymidine phosphorylase to synthesize (halogenated) anticancer and antiviral nucleoside drugs in continuous flow†

Ana I. Benítez-Mateos, Calvin Klein, David Roura Padrosa and Francesca Paradisi *

Received 19th April 2022,
Accepted 8th August 2022

DOI: 10.1039/d2cy00751g

rsc.li/catalysis

Four pharmaceutically relevant nucleoside analogues (5-fluoro-2′-deoxyuridine, 5-chloro-2′-deoxyuridine, 5-bromo-2′-deoxyuridine, and 5-iodo-2′-deoxyuridine) have been synthesized by using a novel thymidine phosphorylase from the halotolerant *H. elongata* (HeTP). Following enzyme immobilization on microbeads, the biocatalyst was implemented as a packed-bed reactor for the continuous production of halogenated nucleosides, achieving up to 90% conversion at the 10 mM scale with 30 min residence time. Taking the synthesis of floxuridine (5-fluoro-2′-deoxyuridine) as a study case, we obtained the highest space–time yield (5.5 g L^{-1} h^{-1}) reported to date. In addition, bioinformatic tools such as MD analysis and CapiPy have contributed to shine light on the catalytic performance of HeTP as well as its immobilization, respectively.

Introduction

Viral infections and cancer disorders are among the most concerning diseases of our society. Nucleoside analogues are classified as an important class of anticancer and antiviral drugs, with many examples already on the market.[1] Specifically, halogenated derivatives have been proven to be very effective therapeutics due to their enhanced solubility and bioavailability.[2] For instance, floxuridine (5-fluoro-2′-deoxyuridine) is effective against different types of cancer and it is also an active substance used in the manufacturing of vaccines against SARS-related coronaviruses.[3–5]

Since the 1950s, nucleoside analogues have been mainly synthesized by chemical strategies which generally require multi-step pathways, hazardous and extreme conditions, and large waste production.[6] More recently, enzymatic synthesis has evolved as an attractive alternative to overcome those issues.[7] Apart from an exquisite substrate selectivity, enzymes are biocompatible and biodegradable catalysts that can work at mild physiological conditions. Although enzymes still suffer from poor substrate solubility and low substrate loading, discovery of more robust enzymes together with state-of-the-art technologies (*i.e.* enzyme immobilization, flow chemistry) bear a high potential towards more sustainable synthesis of nucleoside drugs.[7–9]

Thymidine phosphorylases (TP) (EC 2.4.2.4) are part of the family II of nucleoside phosphorylases and catalyze the cleavage of the glycosidic bond of thymidine in presence of phosphate. TP are highly selective for 2′-deoxy pyrimidine nucleosides while they accept a broad variety of modifications at the C5 position of the nucleobase.[10] These catalytic properties make TP ideal biocatalysts for the two-step production of halogenated thymidine analogues in just one pot (Scheme 1).

Although the biocatalytic synthesis of nucleoside drugs has been thoroughly studied during the last decades with some industrial examples,[11,12] new approaches are still desired to develop scalable enzymatic syntheses.[7] While the biocatalyst's performance can be improved by protein engineering, enzyme discovery, or enzyme immobilization,[13–15] flow chemistry is emerging as a very powerful tool to intensify the process reaction, minimize the waste and bring biocatalysis closer to industrial scale.[16]

Here we present a highly stable thymidine phosphorylase from *Halomonas elongata* (HeTP) as a robust and efficient candidate to synthesize 5-halogenated-2′-deoxyuridines. HeTP

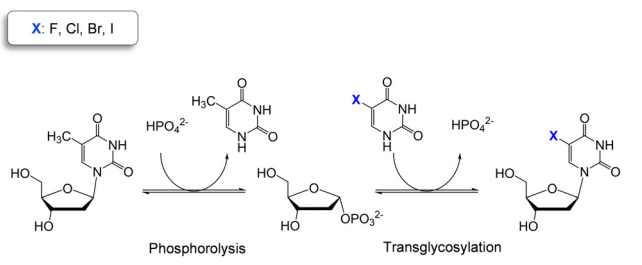

Scheme 1 Two-step one-pot enzymatic reaction for the synthesis of halogenated pyrimidine nucleosides using thymidine as sugar donor.

Department of Chemistry, Biochemistry and Pharmaceutical Sciences, University of Bern, Freiestrasse 3, 3012 Bern, Switzerland. E-mail: francesca.paradisi@unibe.ch

† Electronic supplementary information (ESI) available. See DOI: https://doi.org/10.1039/d2cy00751g

has been characterized in terms of activity and stability against temperature, pH, and presence of organic co-solvent which are often needed during the synthesis of nucleoside analogues. The HeTP biocatalyst was further improved by covalent immobilization on methacrylate microbeads which then allowed its integration into a packed-bed reactor (PBR) for the intensification of the process to synthesize nucleoside drugs under flow conditions. Flow biocatalysis technology as well as *in silico* analyses have been adopted in this work to boost the biocatalytic potential of HeTP. Finally, we have investigated the substrate scope of HeTP towards other pyrimidine nucleoside drugs providing new insights into the active pocket of HeTP.

Results and discussion

Characterization of TP from the halotolerant *H. elongata* (HeTP)

The efficiency and scale-up of synthetic processes are generally linked to high temperatures and presence of co-solvents to which enzymes are not naturally adapted. These conditions are certainly needed to enhance the poor water-solubility of nucleoside analogues. For this reason, we screened the genome of the halotolerant organism *Halomonas elongata* which we have extensively studied in our lab as a source of robust enzymes, with an inherited tolerance towards co-solvents.[17–22] HeTP was expressed in *E. coli* as a soluble enzyme. After optimization of the protein expression (Fig. S1†), HeTP harbouring a (6×)His-tag in the C-terminal was purified by IMAC obtaining 25–35 mg of protein per L of culture media (Fig. S2†).

The activity of HeTP towards the phosphorolysis of thymidine reached 112.8 U mg^{-1} at 70 °C in 0.5 M phosphate buffer at pH 7.0 (Fig. S3†). Interestingly, HeTP presented an increasing activity up to 0.5 M of phosphate, and still retained activity even at 0.9 M phosphate, which may be due to its origin from a halotolerant microorganism (Fig. S3B†). To simplify the reaction set up, the temperature for the standard activity assay was set at 30 °C where HeTP maintains in any case 80% of the initial activity after 6 h (Fig. S4†). Moreover, the enzyme can be stored at 4 °C or room temperature for 2 weeks while retaining most of the activity (Fig. S5†). In terms of pH, HeTP was stable between pH 6.0 and 9.0 for 3 h (Fig. S6†). In addition, HeTP retained 80% of the phosphorolysis activity when 10% of DMSO or MeOH was added to the reaction media (Fig. S7A†). Interestingly, HeTP activity was mostly retained (at least 75%) after incubation in various organic co-solvents such 20% dimethyl sulfoxide (DMSO), 20% methanol (MeOH), 10% ethanol (EtOH), 20% dimethyl formamide (DMF), 10% acetonitrile (MeCN) (Fig. S7B†). While the stability with 20% DMF and 20% MeCN is comparable to the *E. coli* TP, the stability with 20% EtOH is clearly superior to other pyrimidine nucleoside phosphorylases which suffered total loss of activity.[13,23] More comparative analysis could not be conducted due to the lack of previous results for other TPs.

HeTP activity towards different nucleosides

HeTP phosphorolysis towards thymidine, the natural substrate, reached the equilibrium with 62% conversion at 5 mM scale in 2 h (Fig. S8†). The enzyme presented a K_M towards thymidine of 320 μM with a V_{max} of 73 U mg^{-1} (Fig. S9A†). For phosphate, a K_M ~360 μM was estimated (Fig. S9B†). These values are similar to the ones reported for the *E. coli* and human thymidine phosphorylases, while K_M towards thymidine is significantly lower than the TP from *M. hyorhinis* and *T. thermophilus* (473 μM and ~2400 μM, respectively).[15,24–26]

The substrate scope of HeTP towards other natural nucleosides was then probed. As an intrinsic characteristic of the thymidine phosphorylase family, HeTP did not accept purine nucleoside analogues (Table S1†),[10] and it converted only the pyrimidine nucleoside analogues containing a 2′-deoxyribose and the O4 in the nucleobase ring (thymidine or deoxyuridine) (Table S2†). Noteworthy, HeTP did not show activity towards 4′-amino nucleobases which are building blocks for other pharmaceutically relevant nucleosides.[27] In an attempt to shift the activity towards this class of molecules, homology modelling and site-directed mutagenesis to favor the binding of the amino group was carried out (Fig. S10†). Arg171 was identified as a hotspot as it acts as one of the electrostatic stabilizers during the catalysis. Arg171 was replaced by Gln171 and Glu171 which could potentially stabilize the 4-amino moiety, as predicted through docking, MD (molecular dynamics), and amino acid conservation analysis (Fig. S11–S13†). As expected, the substitution R171E led to a loss of activity towards the natural substrate (thymidine),[28] while R171Q showed 10% of activity towards thymidine compared to the wild-type (WT) HeTP. However, none of the variants showed activity towards any of the 4-amino substituted substrates tested despite trying different reaction conditions (Fig. S14, see ESI† for more details).

Biosynthesis of halogenated nucleoside analogues

WT HeTP was applied to the biosynthesis of four 5-substituted nucleoside analogues (5-fluoro-2′-deoxyuridine, 5-chloro-2′-deoxyuridine, 5-bromo-2′-deoxyuridine, and 5-iodo-2′-deoxyuridine) (Scheme 1). Using thymidine as the sugar donor, HeTP was employed to catalyze the one-pot single-enzyme phosphorolysis and transglycosylation of the halogenated nucleoside drugs (Fig. 1). In this first screening, before any optimization of the reaction conditions was carried out, up to 50% of conversion with the four halogenated drugs was achieved in 24 h. Similar conversions were previously achieved for the nucleoside analogues containing F and Br by using 5-fold the amount TP from *E. coli*, but adding half of the sugar donor (thymidine).[13]

Immobilization of HeTP on commercial resins

To improve the efficiency and sustainability of the biocatalytic process, HeTP was immobilized on microparticles that allow the reuse of the biocatalyst as well

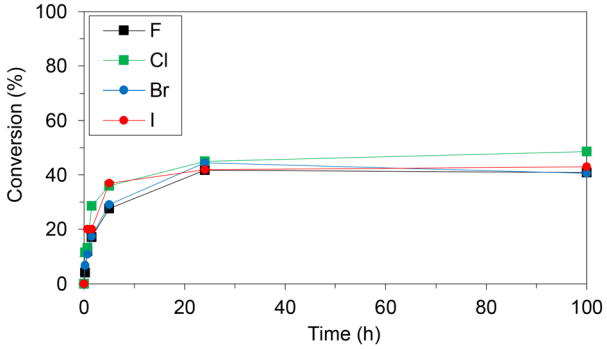

Fig. 1 Monitoring the transglycosylation conversions to produce halogenated nucleoside analogues using free HeTP. The reaction mixture contained 10 mM of the halogenated nucleobase and 4 eq. of thymidine in 20 mM phosphate buffer at pH 7.5. The reactions were triggered with 2 units of free HeTP and incubated at 37 °C and shaking.

as its integration into a continuous reactor. We began testing methacrylate (EP403/S and EP400/SS) and agarose microbeads functionalized either with epoxy and cobalt chelates (Ep/Co^{2+}) or glyoxyl (Gx) groups which are commercial supports and enable the covalent irreversible immobilization of HeTP as observed by SDS-PAGE (Fig. S15†).[29] Although the immobilization yielded more than 85%, the recovered enzymatic activity was low (12–15%) compared to the free enzyme (Table 1). Hence, we decided to explore other supports for enzyme immobilization such as glass microparticles (EziG) and silica microbeads (Si2200). HeTP activity after irreversible immobilization on Si2200 decreased even more (5%). However, the HeTP immobilized on EziG yielded up to 3-fold higher recovered activity (38%) as the enzyme was reversibly bound to the support by metal coordination affinity which maintains the flexibility of the enzyme (Table 1).

Analysis of HeTP using CapiPy,[30] revealed that the C-terminal His-tag is completely exposed and on the backside of the catalytic cleft, hence explaining the high recovered activity when immobilizing only through the (6×)-HisTag (Table 1 and Fig. S16A†). On the other hand, HeTP has 14 solvent-accessible lysines per monomer scattered throughout the surface. Therefore, an irreversible and covalent multipoint attachment could reduce the necessary domain movement for the catalytic activity of HeTP and create a distortion of the protein structure leading to lower recovered activity. Moreover, in the open conformation of the enzyme, multiple lysines in the active site are also accessible and could abolish activity when directly involved in the immobilization (Fig. S16B†).

The reusability of the different immobilized HeTP preparations was then tested. We found that the immobilized HeTP on Gx-EP403/S and Ep/Co-EP403/S retained more than 90% of the initial activity after 10 reaction cycles in batch, while the immobilized HeTP on EziG lost 30–50% of activity after only 5 reaction cycles (Fig. S17†). Therefore, Gx-EP403/S was selected as support for the subsequent studies, considering the recovered activity of the enzyme, the low cost of the support, and the operational stability of the biocatalyst in batch. The protein loading on Gx-EP403/S was also optimized, with 3 mg g^{-1} of HeTP resulting in the best preparation (Fig. S18†).

Enzyme immobilization often enhances the enzyme stability under harsher conditions. Thus, the temperature and DMSO stability of the irreversibly immobilized HeTP was tested. After 24 h of incubation at 30–45 °C, the immobilized HeTP retained more than 85% of the initial activity, while the free enzyme lost up to 50% (Fig. S19†). The stability of HeTP in presence of 10–20% DMSO was also increased after enzyme immobilization as HeTP maintained full initial activity after 3 h (Fig. S20†). Some of these results are comparable to the

Table 1 Immobilization parameters of the HeTP on different supports through various chemistries. The offered enzyme was 1 mg g^{-1}. Immobilization yield: (protein in solution – protein in the supernatant after immobilization)/protein in solution × 100. Recovered activity: specific activity of the free enzyme/specific activity of the immobilized enzyme × 100. Expressed activity: activity of the immobilized enzyme per g of support

Support code	Reactive group	Enzyme-support binding	Matrix material	Immobilization yield (%)	Recovered activity (%)	Expressed activity (U g^{-1})
Ep/Co^{2+}-EP403/S	Epoxy/Co^{2+}	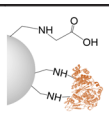	Methacrylate	100	19	11.9
Ep/Co^{2+}-AG	Epoxy/Co^{2+}		Agarose	98	19	12.2
Ep/Co^{2+}-Si2200	Epoxy/Co^{2+}		Silica	65	6	3.2
		Irreversible				
Gx-EP403/S	Aldehyde	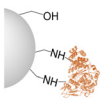	Methacrylate	97	23	20.5
Gx-EP400/SS	Aldehyde		Methacrylate	85	13	10.9
Gx-AG	Aldehyde		Agarose	87	18	11.2
		Irreversible				
EziG1	Fe^{3+}	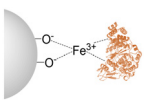	Hydrophilic glass	97	38	35.9
EziG2	Fe^{3+}		Hydrophobic polymer	99	27	25.6
EziG3	Fe^{3+}		Semi-hydrophilic polymer	98	26	25.0
		Reversible				

solvent stability of the immobilized TP from *E. coli*, but only DMF and MeCN were used in that work.[13]

Optimization of the synthesis of halogenated nucleoside analogues with immobilized HeTP

The Gx-EP403/S immobilized HeTP was then applied for the synthesis of floxuridine (5-fluoro-2′-deoxyuridine) as a model reaction due to its relevance as antiviral, antibacterial and anticancer drug. The sugar donor concentration as well as the phosphate buffer were optimized for the transglycosylation. 10 mM phosphate buffer and 10 eq. of sugar donor were selected as the best conditions to reach the maximum conversion (85%) while using the least of reagents (Fig. S21†). Further attempts to improve the conversion by increasing the nucleobase concentration, the amount of biocatalyst, and the temperature were not successful, in agreement with previous studies on nucleoside phosphorolysis (Table S3†).[31] In contrast, the conversion was maintained when the nucleobase concentration was increased up to 20 mM with 10 eq. sugar donor (Table S3†), as it could be expected from the law of mass action considering relative concentrations.[32] To the best of our knowledge, this is the highest substrate concentration used for the enzymatic synthesis of floxuridine reported to date.

With the optimized conditions, we also performed the biosynthesis of the other halogenated nucleoside analogues in batch mode. The transglycosylation conversion reached 70–80% for the Br, I, and Cl nucleoside analogues (Table 2).

Flow biosynthesis of halogenated nucleoside drugs: process intensification

To increase the productivity of the biocatalytic system, the immobilized HeTP was implemented into a packed-bed reactor (PBR) for the continuous biosynthesis of halogenated nucleoside drugs. To do this, the nucleobase and the sugar donor were mixed with a T-tube before entering the PBR. HPLC pumps were used to modulate the flow-rate with residence times (R.T.) from 15 to 45 min, reaching the equilibrium at 30 min of R.T. for the F, Br, and Cl nucleoside drugs (Table 3). To the best of our knowledge, this is the first time that a thymidine phosphorylase is implemented under flow conditions for the synthesis of halogenated nucleoside drugs. In fact, to date, only one study describes the biocatalysed flow synthesis of the F and I analogues but with a different enzyme (2′-deoxyribosyl transferase) immobilized on epoxy silica.[33]

Table 2 Monitoring the biosynthesis of halogenated nucleoside analogues in batch by using the immobilized HeTP. Phosphorolysis of thymidine (%P) and transglycosylation of the nucleoside analogue (%T) are depicted. 20 mg of immobilized HeTP (3 mg g^{-1}) were added to 1 mL of reaction mixture (10 mM nucleobase and 100 mM sugar donor in 10 mM phosphate buffer at pH 7.5) and incubated at 37 °C under shaking

Halogen in nucleobase	2 h		24 h		120 h	
	%P	%T	%P	%T	%P	%T
F	5	33	17	84	18	85
Cl	4	28	14	76	15	79
Br	4	20	10	67	10	70
I	6	35	12	80	12	83

Table 3 Continuous flow biosynthesis of halogenated nucleoside analogues. Phosphorolysis of thymidine (%P) and transglycosylation of the nucleoside analogue (%T) are depicted. The PBR (volume: 2.16 mL) was filled with the immobilized HeTP (3 mg g^{-1}). 10 mM nucleobase and 100 mM thymidine in 10 mM phosphate buffer at pH 7.5 were pumped to the PBR. The flow-rate was adjusted (48–144 μL min^{-1}) to achieve the different residence times depicted. The flow reactions were performed at 37 °C

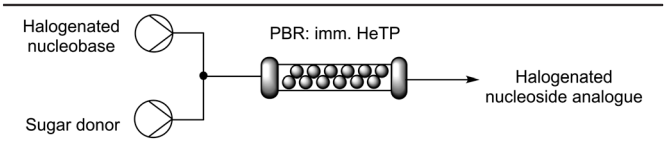

Halogen in nucleobase	15 min		30 min		45 min	
	%P	%T	%P	%T	%P	%T
F	9	53	15	82	15	87
Cl	6	55	14	85	15	86
Br	9	63	14	84	15	88
I	7	55	11	74	13	83

The scale of the flow biosynthesis of floxuridine was increased to 50 mM of the nucleobase while the sugar donor was maintained at 100 mM. Unsurprisingly, the conversion decreased from 87% to 17% while the amount of the final product (8 mM) was maintained (Table S4†). As the nucleobase concentrations used herein are unusually high, a level of inhibition by the nucleobase may be observed, resulting in a slower reaction rate.[15,34] At 20 mM nucleobase with 10 eq. of sugar donor, which is the maximum achievable in terms of water solubility with this set up, 85% conversion was again achieved but in this case the amount of product was 2-fold higher at 16.8 mM (Table S5†). This system provided the highest space–time yield reported to date for the synthesis of floxuridine (Table 4).[13,33,35,36]

In terms of the biocatalyst stability in flow, after 20 column volumes (10 h), more than 60% conversion was maintained (Fig. S22†). These results show a significant improvement over the previously reported example in which just 35% conversion was retained after 10 h.[33] Besides, we stored the PBR at 4 °C for 2 months while not in use, preserving more than 90% of the enzymatic activity.

Table 4 Scale-up flow biosynthesis of halogenated nucleoside analogues. The PBR (volume: 2.16 mL) was filled with the immobilized HeTP (3 mg g^{-1}). 10 eq. of sugar donor (thymidine) were used. R.T. 45 min. Temperature: 37 °C

Nucleobase (mM)	Conversion (%)	STY (g L^{-1} h^{-1})	Catalyst productivity ($mg_{product}$ mg_{enzyme}^{-1} h^{-1})
10	87 ± 1	2.9	0.95
20	84 ± 2	5.5	1.84

Conclusions

We have expanded the toolbox of robust thymidine phosphorylases with the halotolerant HeTP. This is the first time that a thymidine phosphorylase has been implemented in a flow reactor. Moreover, we have pioneered the biosynthesis of 5-chloro-2′-deoxyuridine by using isolated enzymes.[35]

This work also showcases the potential of two key technologies in biocatalysis: enzyme immobilization and flow chemistry. The immobilized HeTP has enhanced stability against high temperatures, co-solvents and long-term storage compared with its free counterpart. Enzyme immobilization also enabled the reuse of the biocatalyst for 10 cycles retaining the full enzymatic activity, which means a decrease in waste and process costs. Finally, continuous flow technology speeds up biosynthetic processes, while offering an automatized and controlled handling of the system. This has allowed the process intensification of floxuridine reaching the highest STY and productivity results reported so far. Hence, our work is timely in progressing the biosynthetic strategies of such important molecules. Specifically with the relevance of floxuridine as anticancer and building block in SARS-related vaccines.

Experimental section

Materials

All chemical reagents were acquired from Sigma Aldrich (Gillingham, UK), Thermo Fisher (Loughborough, UK), Acros Organics (Reinach, Switzerland), or Fluorochem (Hadfield, UK) and used without further purification. Plain agarose (6BCL) was purchased from Agarose Bead Technologies (Madrid, Spain). The methacrylate supports were purchased from Resindion S.R.L (Milan, Italy). The EziG™ (glass microparticles) were kindly donated by EnginZyme.

HeTP expression and purification

The gene *deoA* codifying for the HeTP (A.N. Q7CP66) was cloned into the pET28b plasmid (NcoI/XhoI) and transformed into *E. coli* BL21(DE3) star competent cells by heat-shock at 42 °C. Then, 1 L flasks containing 300 mL of autoinduction medium (ZYM) with 50 μg mL^{-1} kanamycin were inoculated with a colony and incubated at 37 °C for 20 h. Protein expression in LB and TB media were also tested (Fig. S1†). The resulting cells were harvested by centrifugation at 4500 rpm and resuspended in 50 mM phosphate buffer, 300 mM NaCl and 30 mM imidazole at pH 7.0. The suspension was placed on ice and sonicated at 40% amplitude for 8 min, with pulses of 5 s ON, 10 s OFF. After centrifugation at 12 300*g* for 45 min, the supernatant was filtered with a 0.45 μm filter and HeTP was purified from the supernatant by a Ni-NTA column in the AKTA-pure. HeTP was eluted in 50 mM phosphate buffer, 300 mM NaCl and 300 mM imidazole at pH 8.0. The purified enzyme was dialyzed twice in 100 mM phosphate buffer at pH 7.0. The protein expression and purification were analyzed by SDS-PAGE.

Determination of protein concentration

The protein concentration was estimated by measuring the absorbance at 280 nm in the EPOCH2 (nanodrop Tek3 plate) and using the predicted extinction coefficient 14 105 $M \times cm^{-1}$ and the molecular weight 47 736 Daltons obtained from **https://web.expasy.org/protparam**. Low protein concentrations (<1 mg mL^{-1}) were determined by Bradford assay by measuring the absorbance at 595 nm of a solution containing 5 μL of protein sample with 250 μL of Bradford reagent. A standard curve was done with BSA.

Activity assay

A modified photometric assay previously reported was used to assess the activity of the soluble HeTP. Briefly, 990 μL of 1 mM thymidine and 0.5 M potassium phosphate at pH 7.0 were added to a 1 mL-cuvette and the reaction was triggered with 10 μL of HeTP (0.25 mg mL^{-1}). The absorbance at 290 nm was recorded for 2 min at 30 °C. Alternatively, the activity was monitored in a 96-well plate by mixing 300 μL of substrate solution and 5 μL of HeTP (d = 0.75 cm). In the time frame of linear absorbance decrease, regression was performed to calculate the slope of the absorbance decrease per minute. One unit is defined as the amount of enzyme that will convert 1 μmol of thymidine to thymine per minute. The specific enzyme activity (U mg^{-1}) was calculated as reported by Krenitsky *et al.*,[37] based on the difference in millimolar extinction coefficients (ε) between thymidine and thymine which under the assay conditions equals 1. Specific activity was then calculated with eqn (1):

$$\frac{\left(R_{\text{enzyme}} - R_{\text{blank}}\right) \times V_{\text{total}} \times \text{DF}}{\frac{\varepsilon \times V_{\text{enzyme}} \times d}{C_{\text{enzyme}}}} \quad (1)$$

where:
R_{enzyme} = slope of the reaction regression (min^{-1})
R_{blank} = slope of the blank regression (min^{-1})
DF = dilution factor of enzyme
ε = difference in millimolar extinction coefficient between thymidine and thymine (M^{-1} cm^{-1})
V_{enzyme} = volume of enzyme added (mL)
V_{total} = total volume of the reaction (mL)
C_{enzyme} = concentration of the added enzyme solution (mg mL^{-1})
d = pathlength (cm).

Biotransformations in batch mode

Batch reactions with soluble enzyme (2 units) were incubated at 37 °C and under shaking for 24 h in 1 mL of reaction mix containing the sugar donor, the nucleobase, and phosphate buffer at pH 7.0 at the specified concentrations. Batch reactions with immobilized enzyme were triggered adding 50 mg of 3 mg g^{-1} immobilized HeTP, unless otherwise specified. The reactions were monitored by HPLC.

The conversion (%) was calculated from the HPLC analyses of the reaction mixtures following the eqn (2):

$$\frac{\text{product area}}{\text{product area} + \text{substrate area}} \times 100 \quad (2)$$

The molar conversions (%) were also confirmed by using standard curves of the substrates and products (1–50 mM).

Activation of supports and enzyme immobilization

Ep-AG (agarose microbeads activated with epoxy groups). Epoxy-agarose was prepared as previously described.[38] The addition of Co^{2+}-chelates was carried out by incubating 1 g of epoxy-agarose with 2 mL of modification buffer (0.1 M sodium borate, 2 M iminodiacetic acid pH 8.0) for 2 h. After filtration and washing, the support was incubated with 5 mL of metal buffer (30 mg mL^{-1} of $CoCl_2$). After filtration and washing, 5 mL of enzyme solution were added to the Ep/Co^{2+}-AG and the suspension was incubated for 6 h under shaking at room temperature. The immobilized enzyme was washed with 3 mL of desorption buffer (50 mM EDTA, 0.5 M NaCl in 50 mM phosphate buffer, pH 7.2). Finally, the remaining epoxy groups were blocked by incubation with 4 mL of 3 M glycine pH 8.5 overnight and afterwards the immobilized enzyme was washed with 100 mM phosphate buffer at pH 7.5 before its storage.

EP403/S (methacrylate microbeads activated with epoxy groups). EP403/S activated with epoxy groups was commercially available. The addition of Co^{2+}-chelates and the enzyme immobilization were carried out as described in the previous section for Ep-AG.

Ep-Si2200 and Ep-Si250 (silica microbeads activated with epoxy groups). 1 gram of silica microbeads (Sipernat® 2200-PC and Sipernat® 250-PC) were washed and resuspended in 2 mL of H_2O. Then, 0.5 mL of 25% of 3-glycidyloxypropyl trimethoxysilane in acetone were added drop by drop to the previous suspension. The suspension was incubated overnight at 25 °C under shaking. After filtration and washing, the addition of Co^{2+}-chelates and the enzyme immobilization were carried out as described in the previous section for Ep-AG.

Gx-AG (agarose microbeads activated with aldehyde groups). Epoxy-agarose was activated with glyoxyl groups following a modified version of a previous protocol.[39] Briefly, 1 g of epoxy-agarose was incubated with 10 mL of 100 mM H_2SO_4 overnight under orbital shaking. Then, the support was filtered and washed. The resulting glyceryl support was oxidized with 10 mL of 30 mM $NaIO_4$ for 2 h under orbital shaking. After filtration and washing, 10 mL of enzyme solution in 100 mM sodium bicarbonate buffer at pH 10.0 were mixed with 1 g of AG-Gx and incubated under orbital shaking for 3 h at 4 °C. Then, the suspension was filtered and incubated with 10 mL of 1 mg mL^{-1} $NaBH_4$ for 30 min at 4 °C to reduce the imine bonds. The immobilized enzyme was washed with 100 mM phosphate buffer at pH 7.5 before its storage.

Stability tests

HeTP was incubated in 1 mL of buffer. At different time points, 100 μL of enzyme solution/suspension were withdrawn to measure the activity as described above.

Co-solvent stability. The enzyme solution/suspension was incubated at 25 °C for 3 h.

Temperature stability. The enzyme solution/suspension was incubated at 30 °C, 37 °C, or 45 °C for 24 h.

pH stability. The enzyme solution/suspension was incubated at 25 °C for 3 h in Universal buffer (60 mM citric acid, 25 mM sodium tetraborate, 50 mM potassium chloride, 50 mM TRIS, 50 mM potassium phosphate) where the pH was adjusted as required with 0.2 M NaOH.

Flow reactions

Flow biotransformations were performed using a R2S/R4 Vapourtec flow reactor equipped with a V3 pump and an Omnifit glass column (6.6 mm i.d. × 100 mm length) filled with the immobilized enzyme (2 g with 3 mg g^{-1} of protein loading) as a packed-bed reactor (PBR) of 2.4 mL. A first equilibration step was performed by running 10 mM phosphate buffer pH 7.0 at 0.4 mL min^{-1} for 10 min. Then, the solutions of substrates at different concentrations were mixed in a T-tube and pumped through the PBR containing the immobilized biocatalyst. The flow-rate was adapted depending on the desired residence time for each reaction (R.T. 15 min corresponds to 0.160 mL min^{-1}; R.T. 30 min corresponds to 0.080 mL min^{-1}; R.T. 45 min corresponds to 0.053 mL min^{-1}) unless otherwise specified. Samples were collected after each column volume and analyzed by HPLC.

HPLC analysis

The samples were prepared by mixing 100 μL of the reaction medium with 200 μL of MeCN and 200 μL of 0.2% HCl in H_2O (or 400 μL of MeOH). The samples were filtered with a 0.45 μm PTFE filter prior submission to HPLC Dionex UltiMate 3000 (Thermo Fisher, Loughborough, UK) equipped with a C18 column 3.5 μm, 2.1 × 100 mm (Waters, Elstree, UK). 2 μL of sample were injected. For the phosphorolysis analysis, a gradient method 5 : 95 to 95 : 5 (H_2O : MeCN containing 0.1% TFA) over 4 min with a flow rate of 0.8 mL min^{-1} at 45 °C was employed. Thymidine (4 min) and thymine (3.1 min) were detected by UV at 265 nm. For the analysis of both phosphorolysis and transglycosylation, a gradient method 1 : 55 to 55 : 1 (H_2O : MeOH) over 8 min was used. 5′-Azacytosine (1.8 min), 5′-aza-2′-deoxycitidine (2.9 min), were detected by UV at 250 nm. Thymidine (5.1 min), thymine (4.1 min), 5-fluorouracil (2.6 min), and 5-fluoro-2′-deoxyuridine (4.4 min) were detected by UV at 265 nm. 5-Chlororouracil (3.9 min), 5-chloro-2′-deoxyuridine (5.2 min), 5-bromorouracil (4.3 min), 5-bromo-2′-deoxyuridine (5.5 min), 5-iodouracil (5.1 min), and 5-iodo-2′-deoxyuridine (6 min), cytosine (2 min), 2′-deoxycitidine (3.76 min) were detected by UV at 280 nm.

Modelling and docking analysis

HeTP was modelled using SWISS-MODEL *via* the Expasy web server. Visualization of the active site pocket was performed by using the CASTp web server. The resulting PDB file was then loaded into Chimera alongside the original HeTP model

and colored for visualization. The model was used for the docking studies, performed with Autodock Vina.[40] The substrates were manually build using the Build function in UCSF Chimera from their SMILES code.[41] The results were analyzed and visualized in UCSF Chimera and PyMOL.[42]

MD analysis

To perform the molecular dynamics studies, the Enlighten2 plugin for PyMOL was used.[43] Simulations were performed with the monomeric structure of HeTP and with mobility only on the residues at 12 Å surrounding the docked substrate. After minimization of the system, the MD simulation was performed for 1 ns. Results were analyzed using the built-in tools of UCSF Chimera.

Author contributions

F. P. supervised and guided the project. A. I. B. M. and F. P. conceptualized the idea and secured the funding. A. I. B. M. conducted most of the experimental part and wrote the first draft of the manuscript. C. K. carried out the first characterization of the HeTP. D. R. P. performed MD and CapiPy analysis. All the authors discussed the results and agreed to the final version of the manuscript.

Conflicts of interest

There are no conflicts to declare.

Acknowledgements

This project was supported by the SNSF (200021_192274, F.P) and the University of Bern "Seal of Excellence Fund" Postdoctoral Fellowship (SELF19-03 BIORPHANDRUG, A.I.B.M).

References

1 L. P. Jordheim, D. Durantel, F. Zoulim and C. Dumontet, *Nat. Rev. Drug Discovery*, 2013, **12**, 447–464.
2 D. Benedetto Tiz, L. Bagnoli, O. Rosati, F. Marini, L. Sancineto and C. Santi, *Molecules*, 2022, **27**, 1643.
3 W. S. Yeo, R. Arya, K. K. Kim, H. Jeong, K. H. Cho and T. Bae, *Sci. Rep.*, 2018, **8**, 1–10.
4 C. M. Galmarini, *Electron. J. Oncol.*, 2002, **3**, 22–32.
5 HS/CN8 classification reference list for dataset 'EU trade since 2015 of COVID-19 medical supplies', **https://ec.europa.eu/eurostat/documents/6842948/11003521/Corona+related+products+by+categories.pdf**, (accessed 11 April 2022).
6 M. J. Lapponi, C. W. Rivero, M. A. Zinni, C. N. Britos and J. A. Trelles, *J. Mol. Catal. B: Enzym.*, 2016, **133**, 218–233.
7 S. C. Cosgrove and G. J. Miller, *Expert Opin. Drug Discovery*, 2022, **17**, 355–364.
8 F. Kaspar, M. R. L. Stone, P. Neubauer and A. Kurreck, *Green Chem.*, 2021, **23**, 37–50.
9 Y. Ni, D. Holtmann and F. Hollmann, *ChemCatChem*, 2014, **6**, 930–943.
10 S. Kamel, H. Yehia, P. Neubauer and A. Wagner, in *Enzymatic and Chemical Synthesis of Nucleic Acid Derivatives*, ed. J. Fernández-Lucas and M.-J. Camarasa Rius, First, 2019, pp. 1–28.
11 M. A. Huffman, A. Fryszkowska, O. Alvizo, M. Borra-Garske, K. R. Campos, K. A. Canada, P. N. Devine, D. Duan, J. H. Forstater, S. T. Grosser, H. M. Halsey, G. J. Hughes, J. Jo, L. A. Joyce, J. N. Kolev, J. Liang, K. M. Maloney, B. F. Mann, N. M. Marshall, M. McLaughlin, J. C. Moore, G. S. Murphy, C. C. Nawrat, J. Nazor, S. Novick, N. R. Patel, A. Rodriguez-Granillo, S. A. Robaire, E. C. Sherer, M. D. Truppo, A. M. Whittaker, D. Verma, L. Xiao, Y. Xu and H. Yang, *Science*, 2019, **366**, 1255–1259.
12 J. A. McIntosh, T. Benkovics, S. M. Silverman, M. A. Huffman, J. Kong, P. E. Maligres, T. Itoh, H. Yang, D. Verma, W. Pan, H. I. Ho, J. Vroom, A. M. Knight, J. A. Hurtak, A. Klapars, A. Fryszkowska, W. J. Morris, N. A. Strotman, G. S. Murphy, K. M. Maloney and P. S. Fier, *ACS Cent. Sci.*, 2021, **7**, 1980–1985.
13 I. Serra, T. Bavaro, D. A. Cecchini, S. Daly, A. M. Albertini, M. Terreni and D. Ubiali, *J. Mol. Catal. B: Enzym.*, 2013, **95**, 16–22.
14 S. Rocchietti, D. Ubiali, M. Terreni, A. M. Albertini, R. Fernández-Lafuente, J. M. Guisán and M. Pregnolato, *Biomacromolecules*, 2004, **5**, 2195–2200.
15 F. Kaspar, P. Neubauer and A. Kurreck, *ChemBioChem*, 2021, **22**, 1385–1390.
16 A. I. Benítez-Mateos, M. L. Contente, D. Roura Padrosa and F. Paradisi, *React. Chem. Eng.*, 2021, **6**, 599–611.
17 D. Roura Padrosa, A. I. Benítez-Mateos, L. Calvey and F. Paradisi, *Green Chem.*, 2020, **22**, 5310–5316.
18 L. Cerioli, M. Planchestainer, J. Cassidy, D. Tessaro and F. Paradisi, *J. Mol. Catal. B: Enzym.*, 2015, **120**, 141–150.
19 D. Roura Padrosa, Z. Nissar, F. Paradisi and D. M. Reactors, *Catalysts*, 2021, **11**, 520.
20 D. Roura Padrosa, V. De Vitis, M. L. Contente, F. Molinari and F. Paradisi, *Catalysts*, 2019, **9**, 232.
21 A. I. Benítez-Mateos and F. Paradisi, *ChemSusChem*, 2022, **15**, 1–9.
22 M. L. Contente, N. Fiore, P. Cannazza, D. Roura Padrosa, F. Molinari, L. Gourlay and F. Paradisi, *ChemCatChem*, 2020, **12**, 5679–5685.
23 N. Hori, M. Watanabe and Y. Mikami, *Biocatalysis*, 1991, **4**, 297–304.
24 N. G. Panova, C. S. Alexeev, A. S. Kuzmichov, E. V. Shcheveleva, S. A. Gavryushov, K. M. Polyakov, A. M. Kritzyn, S. N. Mikhailov, R. S. Esipov and A. I. Miroshnikov, *Biochemistry*, 2007, **72**, 21–28.
25 J. Vande Voorde, F. Gago, K. Vrancken, S. Liekens and J. Balzarini, *Biochem. J.*, 2012, **445**, 113–123.
26 T. Oh and M. H. El Kouni, *PLoS One*, 2018, **13**, 1–18.
27 L. Zhong, Y. Li, L. Xiong, W. Wang, M. Wu, T. Yuan, W. Yang, C. Tian, Z. Miao, T. Wang and S. Yang, *Signal Transduction Targeted Ther.*, 2021, **6**, 201.
28 E. Mitsiki, A. C. Papageorgiou, S. Iyer, N. Thiyagarajan, S. H. Prior, D. Sleep, C. Finnis and K. R. Acharya, *Biochem. Biophys. Res. Commun.*, 2009, **386**, 666–670.

29 A. I. Benítez-Mateos and M. L. Contente, *Catalysts*, 2021, **11**, 814.
30 D. Roura Padrosa, V. Marchini and F. Paradisi, *Bioinformatics*, 2021, **37**, 2761–2762.
31 F. Kaspar, R. T. Giessmann, P. Neubauer, A. Wagner and M. Gimpel, *Adv. Synth. Catal.*, 2020, **362**, 867–876.
32 C. S. Alexeev, I. V. Kulikova, S. Gavryushov, V. I. Tararov and S. N. Mikhailov, *Adv. Synth. Catal.*, 2018, **360**, 3090–3096.
33 F. Rinaldi, J. Fernández-Lucas, D. de la Fuente, C. Zheng, T. Bavaro, B. Peters, G. Massolini, F. Annunziata, P. Conti, I. de la Mata, M. Terreni and E. Calleri, *Bioresour. Technol.*, 2020, **307**, 123258.
34 F. Kaspar, F. Brandt, S. Westarp, L. Eilert, S. Kemper, A. Kurreck, P. Neubauer, C. R. Jacob and A. Schallmey, *ChemRxiv*, 2022, preprint, DOI: **10.26434/chemrxiv-2022-xjvpw**.
35 C. W. Rivero, C. N. Britos, M. E. Lozano, J. V. Sinisterra and J. A. Trelles, *FEMS Microbiol. Lett.*, 2012, **331**, 31–36.
36 M. B. Méndez, C. W. Rivero, F. López-Gallego, J. M. Guisán and J. A. Trelles, *J. Biotechnol.*, 2018, **270**, 39–43.
37 T. Krenitsky and S. Bushby, *US Pat.*, 4178212, Burroughs Wellcome Co., 1979.
38 C. Mateo, G. Fernández-Lorente, E. Cortés, J. L. Garcia, R. Fernández-Lafuente and J. M. Guisan, *Biotechnol. Bioeng.*, 2001, **76**, 269–276.
39 J. M. Guisán, *Enzyme Microb. Technol.*, 1988, **10**, 375–382.
40 J. Eberhardt, D. Santos-Martins, A. F. Tillack and S. Forli, *J. Chem. Inf. Model.*, 2021, **61**, 3891–3898.
41 E. F. Pettersen, T. D. Goddard, C. C. Huang, G. S. Couch, D. M. Greenblatt, E. C. Meng and T. E. Ferrin, *J. Comput. Chem.*, 2004, **25**, 1605–1612.
42 W. L. Delano, CCP4 Newsl, Protein Crystallogr.
43 K. Zinovjev and M. W. Van Der Kamp, *Bioinformatics*, 2020, **36**, 5104–5106.